TECHNICAL ARTICLE

Improvement in Modal Testing Measurements by Modeling and Identification of Shaker–Stinger–Structure Interactions

M. Mohammadali and H. Ahmadian

Center of Excellence in Experimental Solid Mechanics and Dynamics, School of Mechanical Engineering, Iran University of Science and Technology, Narmak, Tehran 16844, Iran

Keywords
Shaker, Stinger, Shaker Structure Interactions, Dynamic Stiffness Matrix, Frequency Response Function

Correspondence
M. Mohammadali,
Center of Excellence in Experimental Solid Mechanics and Dynamics
School of Mechanical Engineering
Iran University of Science and Technology
Narmak
Tehran 16844
Iran
Email: mohammadali@iust.ac.ir

Received: June 5, 2012;
accepted: May 12, 2013

doi:10.1007/s40799-016-0009-9

Abstract

When a shaker (or exciter) connects to a structure under test (SUT), the dynamic characteristics of the excitation system (shaker, stinger, and transducers) becomes coupled with those of the SUT. These couplings contaminate recorded measurements, especially while exciting light/flexible SUTs. The aim of this work is to consider interactions between excitation system and the SUT and introduce a new analytical model for prediction and hence reducing this systematic error. With the aid of this model, changes in dynamic stiffness of the SUT are estimated based on stiffness of the excitation system. The effects of excitation system location and stiffness are shown in modal testing on a free–free beam. Furthermore, influence of force transducer location is studied in the excitation system setup. The proposed method is successfully used for identification and prediction of excitation system effects on dynamic characteristics of the beam.

Introduction

The purpose of modal testing is to provide an adequate estimate of a SUT model. To this end, impact and shaker excitation techniques are usually used, and each one has its own attributes. Impact testing has consistency problems with input magnitudes and direction besides excitation bandwidth and mixing windows for signal processing. Moreover, impact testing usually overdrives the SUT and excites its nonlinear characteristics, which leads to erroneous measured data. However, while using an exciter, there is much better control on the excited frequency ranges and the level of force (in different frequencies) transmits to the SUT. As a result, exciter testing tends to lead to higher-quality measurements over greater bandwidths.[1]

Basically, a successful modal testing requires: (1) reliable inputs from sensors; (2) use of robust modal data analysis techniques. Some factors behind practical aspects of excitation system setup may cause to record impure measurements. During the vibration under unidirectional loading, The SUT at the excitation point may have DOFs besides the loading direction. This is because of vibration mode shapes, location and direction of loading as well as suspension (especially when suspension is soft). A shaker applies axial force to the SUT, and its armature is designed to have the freedom to move in its axial direction only. If the shaker is connected directly to the SUT, it will constrain the SUT's tendencies to rotate and move in nonaxial DOFs at the junction point. This resistance at the driving point applies an undesired moment(s) and/or force(s) on nonaxial DOFs of the SUT. These phenomena, which called shaker–structure interactions, will show up as systematic errors in acquired measurements.[2]

Piano wire is a method rarely used to link a shaker to the SUT. This type of attachment decouples the conjoined structures in all DOFs (the interaction between the exciter and the SUT in nonaxial directions is removed). In order to transfer excitation force, the axial stiffness of the wire provides through a preload. This preload is normally on the magnitude of three to four times the range of the alternating load.

Typically, both the test structure and shaker must be fixed in order to keep tension on the wire. Therefore, alignment of shaker and SUT becomes an issue.[1]

Another common method to reduce mentioned interactions and measure exerted force to the SUT is to mount force transducer directly on the SUT and employ a stinger (long slender element) between the shaker and the force transducer to transmit force to the SUT. Attaching the force transducer to the SUT can only decouple the SUT's vibrations in the axial direction of the excitation system. Therefore, the stinger should have high axial stiffness but low lateral and bending stiffness in order to excite the SUT axially and to minimize interactions in all nonaxial DOFs.

Many experts[3–9] investigated the shaker–stinger–structure interactions and try to reduce its effects by changing excitation location and/or type and size of stinger. These studies lead to general guidelines depending on SUT, frequency range of interest, level of exerted force and type of suspension. For light SUT, Anderson[5] suggested to mount a force transducer or impedance head on the shaker's armature. He showed employing this technique improves the measurement quality as it prevents the axial resonance of the stinger. Afterwards, this technique was used for testing on an ultra-lightweight, ultraflexible SUT by Ruggiero et al.[10] Ashory and Hajighorbani[11] proposed a model which includes the effect of the rigid body modes of the shaker–stinger–structure system in low frequency ranges. Mayer and Gomez[12] addressed some of major challenges of using a shaker, including the interaction between shaker and the SUT, with the goal of achieving an adequate linear estimate of the SUT model.

Recently, Cloutier et al.[1] studied and presented the effects of alignment, location, length and type of stinger on measured data on a test subject. Avitabile[13] briefly explained some practical aspects of shaker testing. He concluded that there is not a clear answer to which stinger configuration leads to the optimal results, and it depends on the SUT and the frequency range of interest. Moreover, Warren and Avitabile[14] used several test setup configurations to show the effects of single shaker versus multiple shaker as well as stinger type on measured response and extracted mode shapes. The common problems associated with setup of the shakers, stingers, and transducers and resulting measurement errors are reviewed by Peres et al.[2] and Peres and Bono[15] in two related studies.

These studies discuss the quality of shaker–stinger attachment effects on a SUT. However, there is a lack of an analytical formulation which models the interactions between excitation system and the SUT. Accordingly, the quantity of these effects on the recorded measurements is not evaluated numerically. In this article, the main goal is to construct an analytical model for shaker–stinger–structure system. The presented model is developed using the SUT and excitation system dynamic stiffness matrices.

Using two different excitation system setups, a free–free beam is excited at three different points on a wide frequency range, and dynamic responses are measured. The recorded characteristics are compared with the beam model. Next, dynamic stiffness of the excitation system is successfully identified via the introduced analytical model. Eventually, with comparisons of experimental and analytical results, errors caused by the excitation are determined.

The Shaker–Stinger–Structure Model

A SUT (S) and an excitation system (E) setup are shown in Fig. 1. These two systems are attached together at node p with n DOFs. $\mathbf{S}^{[S]}(\omega)$ and $\mathbf{Z}^{[S]}(\omega)$ are global dynamic stiffness matrix of the SUT with m nodes and dynamic stiffness matrix of the excitation system at node p, respectively (see Appendix I). As every field parameter in this work is transferred into the frequency domain, the ω argument is omitted henceforth for simplicity.

The electromagnetic force, the only external force exerted to the set of the SUT and the excitation system, applies to the shaker's armature at node o. Also, the transmitted internal force at node p can be assumed as two opposite external forces, $\mathbf{f}^{[E_p]}$ and $\mathbf{f}^{[S_p]}$ (see Fig. 1). Using Eqs. (A1) and (A4) the motion equations of the SUT and exciter system may be written in the form:

$$\mathbf{f}^{[S]} = \mathbf{S}^{[S]}\mathbf{x}^{[S]} \tag{1}$$

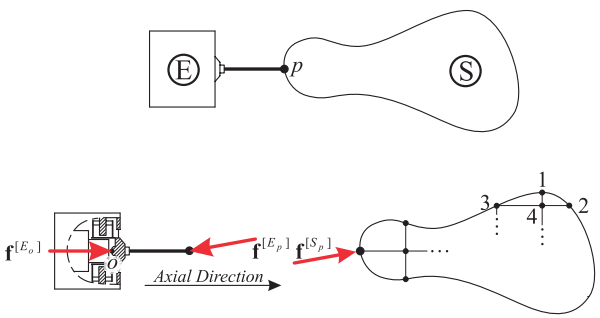

Figure 1 SUT and excitation system models.

in which:

$$\mathbf{S}^{[S]} = \begin{bmatrix} \mathbf{S}^{[S_{11}]} & \mathbf{S}^{[S_{12}]} & \dots & \mathbf{S}^{[S_{1m}]} \\ \mathbf{S}^{[S_{21}]} & \mathbf{S}^{[S_{22}]} & \dots & \mathbf{S}^{[S_{2m}]} \\ \vdots & \vdots & \ddots & \vdots \\ \mathbf{S}^{[S_{m1}]} & \mathbf{S}^{[S_{m2}]} & \dots & \mathbf{S}^{[S_{mm}]} \end{bmatrix}$$

$$\mathbf{x}^{[S]} = \left\{\mathbf{x}^{[S_1]}, \mathbf{x}^{[S_2]}, \dots, \mathbf{x}^{[S_m]}\right\}^{\mathrm{T}}$$

$$\mathbf{f}^{[S]} = \left\{\mathbf{f}^{[S_1]}, \mathbf{f}^{[S_2]}, \dots, \mathbf{f}^{[S_m]}\right\}^{\mathrm{T}}$$

$$\mathbf{f}^{[S_i]} = \{\mathbf{0}\}_{n\times 1}, \quad i \neq p$$

$$\mathbf{f}^{[E_p]} = \mathbf{Z}^{[E_p]}\mathbf{x}^{[E_P]} - \mathbf{Z}^{[E_p]}\mathbf{H}^{[E_{po}]}\mathbf{f}^{[E_o]} \tag{2}$$

$$f^{[S_p]} = -f^{[E_p]} \tag{3}$$

where $\mathbf{S}^{[S_{ij}]}$ is the dynamic stiffness matrix between nodes i and j, $\mathbf{f}^{[S_i]}$ and $\mathbf{x}^{[S_i]}$, respectively, are external force and motion vectors at node i, $\mathbf{x}^{[p]} = \mathbf{x}^{[S_P]} = \mathbf{x}^{[E_P]}$ are motion vectors at node p and $\mathbf{H}^{[E_{po}]}$ is the dynamic flexibility matrix between nodes p and o. Without losing generality of the model, first degree of freedom at nodes p and o is assumed to be in axial direction of the exciter. Therefore, the electromagnetic force, $\mathbf{f}^{[E_o]}$, ideally can be written in the form:

$$\mathbf{f}^{[E_o]} = \left\{f_1^{[E_o]}, 0, \dots, 0\right\} \tag{4}$$

The motions and forces in axial direction of the excitation system have very little interaction with other DOFs at nodes p and o. Regardless of those interactions; the axial DOFs at these nodes decoupled from nonaxial DOFs. Therefore, $\mathbf{Z}^{[E_p]}$ and $\mathbf{H}^{[E_{po}]}$ had the following properties:

$$\begin{aligned} Z_{1i}^{[E_p]} &= Z_{i1}^{[E_p]} = 0 \\ H_{1i}^{[E_{po}]} &= H_{i1}^{[E_{po}]} = 0 \end{aligned} \quad i \neq 1 \tag{5}$$

The amount of exerted force in axial direction at node p, $f_1^{[S_p]}$, is usually known via a force transducer. By incorporating Eqs. (2) and (3), the unknown parts of transmitted force may be written in matrix form:

$$\begin{aligned} \mathbf{f}^{[S_p]} &= \bar{\mathbf{I}}\mathbf{f}^{[S_p]} + \hat{\mathbf{I}}\mathbf{f}^{[S_p]} \\ \bar{\mathbf{I}}\mathbf{f}^{[S_p]} &= -\bar{\mathbf{I}}\left(\mathbf{Z}^{[E_p]}\mathbf{x}^{[p]} - \mathbf{Z}^{[E_p]}\mathbf{H}^{[E_{po}]}\mathbf{f}^{[E_o]}\right) \end{aligned} \tag{6}$$

where $\hat{I}_{ij} = \delta_{i1}\delta_{j1}$ and $\bar{I}_{ij} = \delta_{ij} - \delta_{i1}\delta_{j1}$ $(\bar{I}_{ij} + \hat{I}_{ij} = \delta_{ij})$, hence δ_{ij} is Kronecker's delta. The only nonzero element of $\hat{\mathbf{I}}\mathbf{f}^{[S_p]}$ is $f_1^{[S_p]}$, which is known from measurement. Applying Eq. (5), the above equation can be simplified as:

$$\begin{aligned} \bar{\mathbf{I}}\mathbf{f}^{[S_p]} &= -\bar{\mathbf{I}}\mathbf{Z}^{[E_p]}\mathbf{x}^{[p]} \\ \bar{\mathbf{I}}\mathbf{Z}^{[E_p]}\mathbf{H}^{[E_{po}]}\mathbf{f}^{[E_o]} &= \{\mathbf{0}\}_{n\times 1} \end{aligned} \tag{7}$$

After substituting Eqs. (6) and (7) in pth row of Eq. (1) and simplifying, one obtains:

$$\sum_{i=1}^{m}\mathbf{S}^{[S_{pi}]}\mathbf{x}^{[i]} = \mathbf{f}^{[S_p]} = -\bar{\mathbf{I}}\mathbf{Z}^{[E_p]}\mathbf{x}^{[p]} + \hat{\mathbf{I}}\mathbf{f}^{[S_p]}$$

$$\left(\mathbf{S}^{[S_{pp}]} + \bar{\mathbf{I}}\mathbf{Z}^{[E_p]}\right)\mathbf{x}^{[p]} + \sum_{\substack{i=1 \\ i\neq p}}^{m}\mathbf{S}^{[S_{pi}]}\mathbf{x}^{[i]} = \hat{\mathbf{I}}\mathbf{f}^{[S_p]} \tag{8}$$

By replacing Eq. (8) in pth row of Eq. (1), the motion equation written in matrix form:

$$\begin{aligned} \widetilde{\mathbf{f}}^{[S]} &= \widetilde{\mathbf{S}}^{[S]}\mathbf{x}^{[S]} \\ \widetilde{\mathbf{S}}^{[S_{ij}]} &= \mathbf{S}^{[S_{ij}]} + \bar{\mathbf{I}}\mathbf{Z}^{[E_p]}\delta_{pi}\delta_{pj} \\ \widetilde{\mathbf{f}}^{[S_i]} &= \{\mathbf{0}\}_{n\times 1} + \hat{\mathbf{I}}\mathbf{f}^{[S_p]}\delta_{pi} \end{aligned} \tag{9}$$

where $\widetilde{\mathbf{S}}^{[S]}$ is modified global dynamic stiffness matrix of SUT. The only differences between $\widetilde{\mathbf{S}}^{[S]}$ and $\mathbf{S}^{[S]}$ are at pp elements $(\widetilde{\mathbf{S}}^{[S_{pp}]} = \mathbf{S}^{[S_{pp}]} + \bar{\mathbf{I}}\mathbf{Z}^{[E_p]})$ and the other elements are the same. Instead of using the global dynamic stiffness matrix of SUT in Eq. (8), the dynamic stiffness of SUT at node p, $\mathbf{Z}^{[S_p]}$, can be used and with the same procedure one may obtain:

$$\begin{aligned} \hat{\mathbf{I}}\mathbf{f}^{[S_p]} &= \widetilde{\mathbf{Z}}^{[S_p]}\mathbf{x}^{[p]} \\ \widetilde{\mathbf{Z}}^{[S_p]} &= \mathbf{Z}^{[S_p]} + \bar{\mathbf{I}}\mathbf{Z}^{[E_p]} \end{aligned} \tag{10}$$

where $\widetilde{\mathbf{Z}}^{[S_p]}$ is modified dynamic stiffness of SUT at node p. Modifications in motion Eqs. (9) and (10) are as a result of the attached excitation system to the SUT, and they cause deviation of the SUT dynamic characteristics from uncontaminated one. For reduction or prediction of these deviations generally three methods may be pronounced in the frequency range of interest as follows:

- Reduction of $\bar{\mathbf{I}}\mathbf{Z}^{[E_p]}$ with respect to $\mathbf{S}^{[S_{pp}]}$.
- Increase of $\mathbf{S}^{[S_{pp}]}$ with respect to $\bar{\mathbf{I}}\mathbf{Z}^{[E_p]}$.
- Identification of $\bar{\mathbf{I}}\mathbf{Z}^{[E_p]}$.

A common recommendation to achieve the goal of the first method is to employ a flexible stinger. There is a phenomenon, other than the buckling and axial resonance of the stinger, which limits the stinger flexibility. This phenomenon is missed in the above guidelines and will be clarified later. The second method objective can be obtained by changing the excitation point to a stiffer location of the SUT. Nodes of the SUT in nonaxial direction of the excitation system are the best choice. The third method probably can resolve the problem, and the SUT characteristics can be extracted from measurements. The accuracy of this method depends

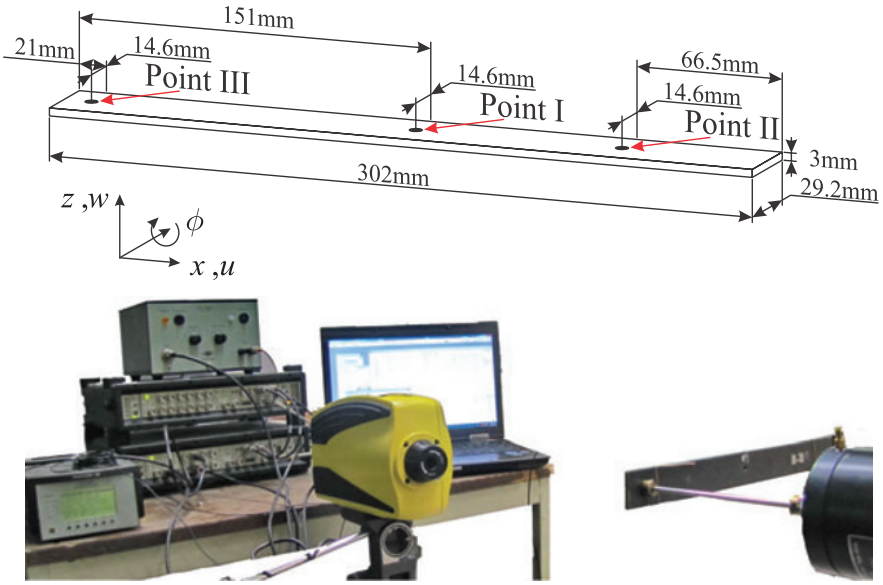

Figure 2 The SUT setup and dimensions.

on correctness of the identified matrix, $\bar{\mathbf{I}}\mathbf{Z}^{[E_P]}$. In the following, effects of these three methods are studied on recorded data from testing on free–free beam.

Experimental Case Study

A steel beam (shown in Fig. 2) is suspended by two narrow stings to simulate free–free boundary condition.

A stinger with length of 12 cm and cross section diameter of 3.5 mm is used for connecting shaker to the SUT. For investigation of force transducer position effect, two excitation system setups, α and β, are defined (see Fig. 3). The α setup composed of a mounted force transducer on the SUT is adjoined to the shaker via the singer. In the β setup, force gage which placed on the shaker's table is linked to the SUT by stinger. Excitation system is connected to the SUT at three different points, called I, II, and III (see Fig. 2), and direct point response at these locations are recorded.

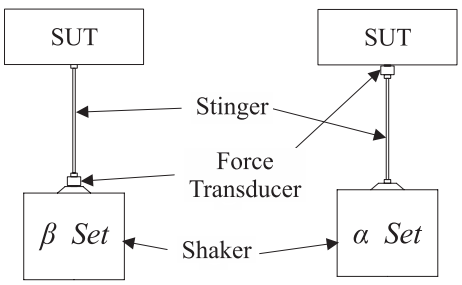

Figure 3 α and β setups of the excitation systems.

Modeling and Discussion

The direct point measurement was done at locations I, II, and III and the recorded FRFs are shown in Fig. 4 (see Appendix II).

The recorded FRFs of α and β setups for excitation at point I are identical. Point I is a node for all torsional and even bending mode shapes. Furthermore, for all odd bending mode shapes, this point only moves in z-axis direction (node for other DOFs). Therefore, in Eq. (8), $\bar{\mathbf{I}}\mathbf{Z}^{[E_P]}\mathbf{x}^{[P]}$ is equal to 0 for all odd bending modes. Consequently, the excitation system attached to point I is ineffective on the dynamic characteristics of the SUT. Additionally, two recorded results at point I reveal that ''motion in the axial direction of the excitation system decoupled from its other DOFs''.

For comparisons of pure SUT responses with measured ones, a theoretical model of the SUT based on Timoshenko beam theory is constructed. Young's modulus of the SUT identified with minimizing the differences between natural frequencies extracted from β set measurements at point I with corresponding natural frequencies of the model.

Hence only bending modes of the beam are excited in this study, for modeling the SUT three DOFs are considered. Using benefits of spectral elements, local dynamic stiffness matrices at point I, II, and III are constructed as:

$$\mathbf{Z}^{[S_X]} = \begin{bmatrix} Z_{ww}^{[S_X]} & Z_{w\phi}^{[S_X]} & 0 \\ Z_{\phi w}^{[S_X]} & Z_{\phi\phi}^{[S_X]} & 0 \\ 0 & 0 & Z_{uu}^{[S_X]} \end{bmatrix}$$
$$\bar{\mathbf{I}}\mathbf{f}^{[S_X]} = \left\{ f_1^{[S_X]} \quad 0 \quad 0 \right\}^{\mathrm{T}} \qquad (11)$$
$$\mathbf{x}^{[X]} = \left\{ w^{[X]} \quad \phi^{[X]} \quad u^{[X]} \right\}^{\mathrm{T}}$$

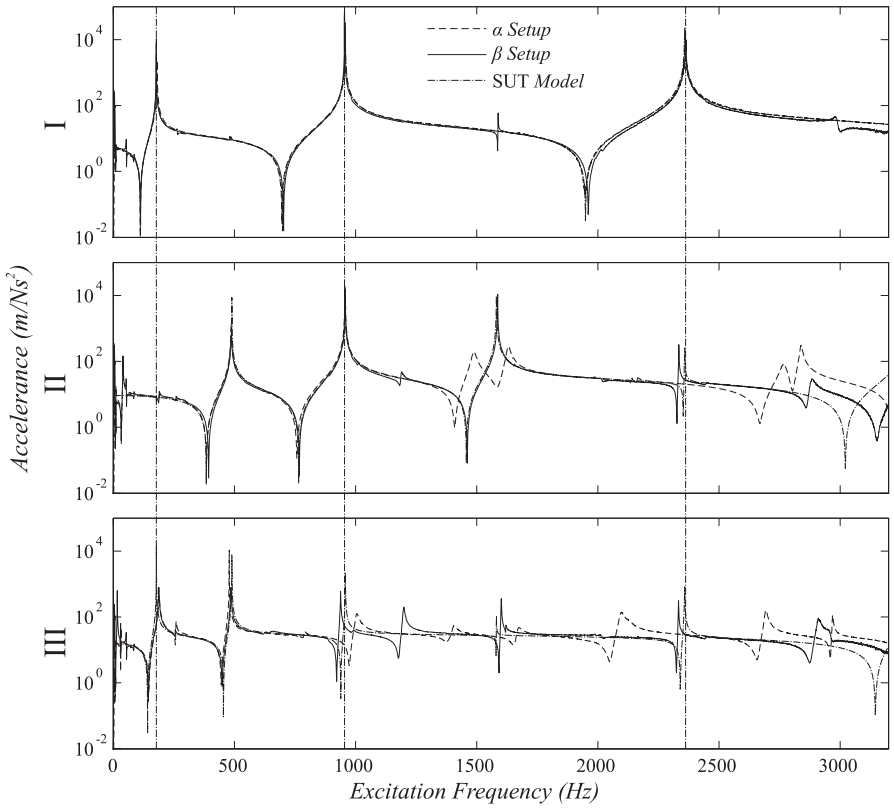

Figure 4 Measured FRFs at points I, II, III and FRFs of the SUT model.

where X is I, II, or III. This model is used to calculate the direct point FRFs of the SUT at points I, II, and III. As can be seen in Fig. 4, recorded FRFs at points II and III are inconsistent with the SUT model. These dissimilarities increase at higher frequencies.

Nevertheless, the β setup test results are more correlated with the SUT model. As a result, the excitation system of β setup has fewer effects than α setup on the dynamic characteristics of the SUT. Also point II is stiffer than point III of the SUT, not always but almost always; therefore, test results at point II are more compatible with theory. Point III is near the free edge of the SUT, and this phenomenon was predictable.

The recorded data with α setup in frequencies higher than 1 kHz is dissimilar to theory results, and their resonances cannot be related. The dominant difference, between theory and experimental data recorded with β setup, takes place near frequencies of 1200 and 2900 Hz. At those frequencies in experimental data, two resonances occur that they are absent in the SUT model; therefore, those are caused by the excitation system of β setup.

For prediction and study the effects of the excitation system of β setup, a model is constructed for it (see Fig. 5). Stinger, which is free on one side (this side will be connected to the SUT) and is connected to the mounted force transducer on the shaker's table from another side, is modeled as an elastic beam (Timoshenko theory). The dynamic characteristics of shaker and the effects of its suspension are not usually known. The equivalent effect of these phenomenon at the force transducer adjoin is modeled with unknown mass and stiffness matrices, **M** and **K**, respectively.

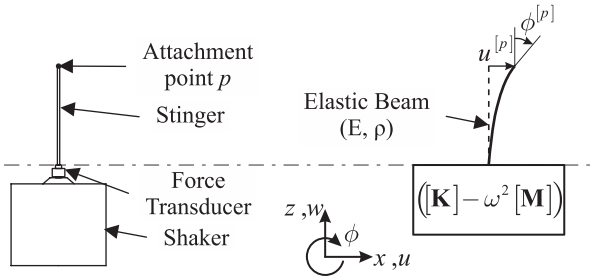

Figure 5 The excitation system model.

As explained in theory section, the SUT response is uninfluenced by the axial stiffness of the excitation system. Furthermore, the axial vibration of the excitation system, as concluded, is decoupled from vibration in other DOFs. Therefore, axial vibration of the excitation system is neglected in modeling of

its motion. Accordingly, **M** and **K** are assumed to be symmetric in the form of:

$$\mathbf{K} = \begin{bmatrix} K_{\phi\phi} & K_{\phi u} \\ K_{u\phi} & K_{uu} \end{bmatrix} \qquad \mathbf{M} = \begin{bmatrix} M_{\phi\phi} & M_{\phi u} \\ M_{u\phi} & M_{uu} \end{bmatrix} \tag{12}$$

where u and ϕ are in lateral and rotational direction shown in Fig. 5. Since internal damping of the shaker causes energy dissipation, elements of **K** are assumed to be complex. Using spectral elements, $\bar{\mathbf{I}}\mathbf{Z}^{[E_p]}$ is constructed in the form of:

$$\bar{\mathbf{I}}\mathbf{Z}^{[E_p]} = \begin{bmatrix} 0 & 0 & 0 \\ 0 & Z_{\phi\phi}^{[E_p]} & Z_{\phi u}^{[E_p]} \\ 0 & Z_{u\phi}^{[E_p]} & Z_{uu}^{[E_p]} \end{bmatrix} \tag{13}$$

By applying Eqs. (11) and (13) to Eq. (10) the modified dynamic stiffness of the SUT may be obtained as below:

$$\begin{aligned} \widehat{\mathbf{I}}\mathbf{f}^{[S_X]} &= \widetilde{\mathbf{Z}}^{[S_X]}\mathbf{x}^{[X]} \\ \widetilde{\mathbf{Z}}^{[S_X]} &= \mathbf{Z}^{[S_X]} + \bar{\mathbf{I}}\mathbf{Z}^{[E_p]} \end{aligned} \tag{14}$$

This model will be called modified SUT (MSUT) model. According to the purpose of matching measured FRFs by β setup with FRFs of the MSUT model, the six unknown elements in Eq. (12) are identified. The objective function is defined as the difference between those two FRFs around their natural frequencies. The identification is done by the combination of random search and gradient methods. The FRFs of the MSUT model is shown in Fig. 6.

Figure 6 shows the FRFs of the MSUT model represent the measured data with better agreements within frequency range of interest. The MSUT model predicts the two resonances picks near 1200Hz and 2900Hz, while the SUT model fails to do so. The smallest non-zero singular value of $\bar{\mathbf{I}}\mathbf{Z}^{[E_p]}$ matrix, Σ_1, is shown in Fig. 6. Near the frequencies, Σ_1 reaches its local maximum values; the excitation system will be in stiffest condition, and when Σ_1 reaches its local minimum (0), the excitation system will be in lateral resonance condition.

The SUT model fails to predict the measured FRFs in vicinity of the excitation frequencies that Σ_1 reaches its local maximum value. At these situations point p does not move laterally and becomes a node in nonaxial direction. It is known in direct measured FRFs an antiresonance point falls between each two resonance peaks. Consequently, one may conclude that, between each two resonances, there is a frequency which at that frequency Σ_1 will reach its local maximum. Therefore, placing a force transducer (or adding mass) at the point p (see Fig. 5), increases the dynamic stiffness of excitation system,

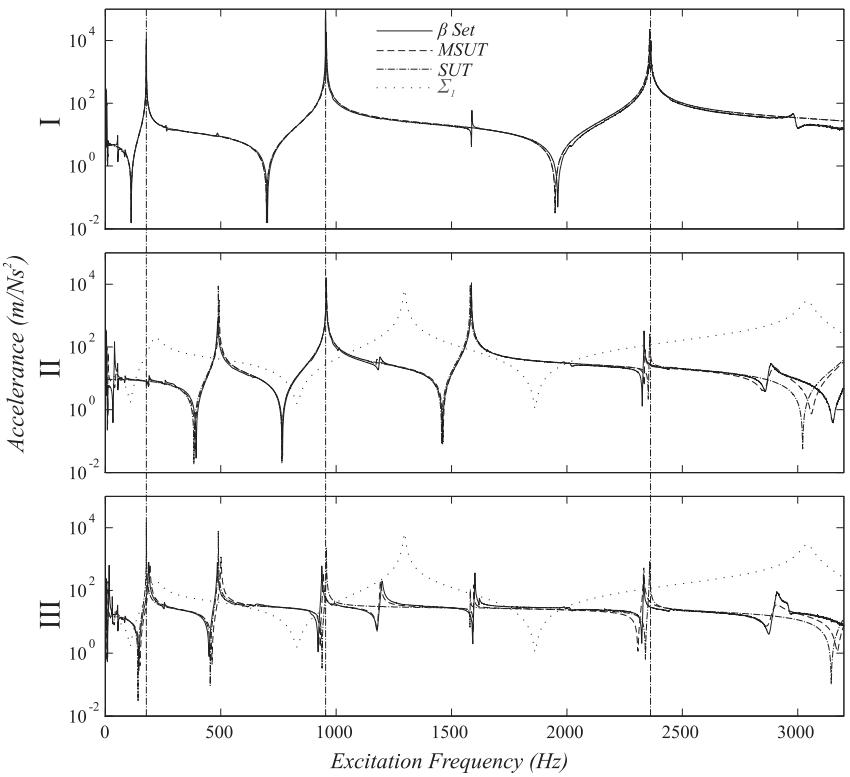

Figure 6 The measured FRFs of the β setup, the SUT and the MSUT models.

and consequently, increases the number of natural frequencies of the excitation system in the frequency range of interest. In this situation, the number of frequencies Σ_1 reaches its maximum values will increase in the measured frequency range, and the measurement errors will increase. For that reason, the inconsistency between α setup and SUT model is due to placing the force transducer at point p.

Conclusions

In this article, effects of the excitation system on the dynamic characteristic of the SUT are studied. The general analytical model refers to SUT and excitation system has been established. Moreover, deviation of dynamic responses of the SUT caused by connection of the excitation system has been predicted. Based on current investigation, the least deviation is around the lateral natural frequencies of the excitation system. Furthermore, between each two of these resonances, supreme deviation in measurement will occur. Therefore, one way to reduce measurement errors is to limit the number of lateral excitation system resonances in the frequency range of interest. This can be accomplished by placing the force gage on the shaker's table and/or decreasing the length of stinger. Using a longer stinger does not necessarily reduce the shaker and SUT interactions. Finally, using the introduced model, extraction of dynamic characteristics of any SUT is possible by modal testing when shaker dynamic properties (mass and stiffness matrices) are already identified and the shaker suspension has not changed.

References

1. Cloutier, D., Avitabile, P., Bono, R., and Peres, M., ''Shaker/Stinger Effects on Measured Frequency Response Functions,'' *Proceedings of the 27th International Modal Analysis Conference*, Orlando, FL, pp. 9–12 (2009).
2. Peres, M.A., Bono, R.W., and Brown, D.L., ''Practical Aspects of Shaker Measurements for Modal Testing,'' *Proceedings of the ISMA2010*, pp. 2539–2550 (2010).
3. Mitchell, L., and Elliott, K., ''How to Design Stingers for Vibration Testing of Structures,'' *Sound and Vibration* **18**(4): 14–18 (1984).
4. Mitchell, L., and Elliott, K., ''A Method for Designing Stingers for Use in Mobility Testing,'' *Proceedings of the 2nd International Modal Analysis Conferences*, pp. 872–876 (1984).
5. Anderson, I., ''Avoiding Stinger Rod Resonance Effects on Small Structures,'' *Proceedings of the 8th International Modal Analysis Conference*, pp. 673–678 (1990).
6. Lee, J.C., and Chou, Y.F., ''The Effects of Stingers on Modal Testing,'' *Proceedings of the 11th International Modal Analysis Conference*, pp. 293–299 (1993).
7. Lee, J.-C., and Chou, Y.-F., ''The Effects of Stingers on Receptance Function Measurements,'' *Journal of Vibration and Acoustics* **118**(2): 220 (1996).
8. McConnell, K., ''Transducer Inertia and Stinger Stiffness Effects on FRF Measurements,'' *Mechanical Systems and Signal Processing* **14**(4): 625–636 (2000).
9. McConnell, K.G., ''Modal Testing,'' *Philosophical Transactions of the Royal Society A: Mathematical, Physical and Engineering Sciences* **359**(1778): 11–28 (2001).
10. Ruggiero, E.J., Tarazaga, P.A., and Inman, D.J., ''Modal Analysis of an Ultra-Flexible, Self-Rigidizing Toroidal Satellite Component,'' *Proceedings of 2004 ASME International Mechanical Engineering Congress and Exposition*, Anaheim, CA, pp. 13–19 (2004).
11. Ashory, M.R., and Hajighorbani, R.A., ''The effects of stingers on measured FRFs,'' *ISMA* **2002**: 2247–2256 (2002).
12. Mayes, R.L., and Gomez, A.J., ''Part 4: What's Shakin', Dude? Effective Use of Modal Shakers,'' *Experimental Techniques* **30**(4): 51–61 (2006).
13. Avitabile, P., ''Can the Shaker Stinger Have Any Effect on the Frequency Response Measurements?,'' *Experimental Techniques* **34**(3): 11–12 (2010).
14. Warren, C., and Avitabile, P., ''Effects of Shaker Test Set Up on Measured Natural Frequencies and Mode Shapes,'' *28th IMAC, A Conference on Structural Dynamics*, pp. 1245–1250 (2011).
15. Peres, M.A., and Bono, R.W., ''Modal Testing Excitation Guidelines,'' *Sound and Vibration* **45**(11): 8–12 (2011).

Appendix I

A structure with m nodes and n DOFs at each node is considered as shown in Fig. A1. External force vector, $\mathbf{f}$, and displacement vector, $\mathbf{x}$, in the frequency domain, can be related by global dynamic stiffness matrix of structure, $\mathbf{S}$, in the form:

$$\mathbf{f} = \mathbf{S}\,\mathbf{x} \tag{A1}$$

in which

$$\mathbf{S} = \begin{bmatrix} \mathbf{S}^{[11]} & \mathbf{S}^{[12]} & \dots & \mathbf{S}^{[1m]} \\ \mathbf{S}^{[21]} & \mathbf{S}^{[22]} & \dots & \mathbf{S}^{[2m]} \\ \vdots & \vdots & \ddots & \vdots \\ \mathbf{S}^{[m1]} & \mathbf{S}^{[m2]} & \dots & \mathbf{S}^{[mm]} \end{bmatrix} \tag{A2}$$

$$\mathbf{f} = \left\{\mathbf{f}^{[1]}, \mathbf{f}^{[2]}, \dots, \mathbf{f}^{[m]}\right\}^{\mathrm{T}}$$

$$\mathbf{x} = \left\{\mathbf{x}^{[1]}, \mathbf{x}^{[2]}, \dots, \mathbf{x}^{[m]}\right\}^{\mathrm{T}}$$

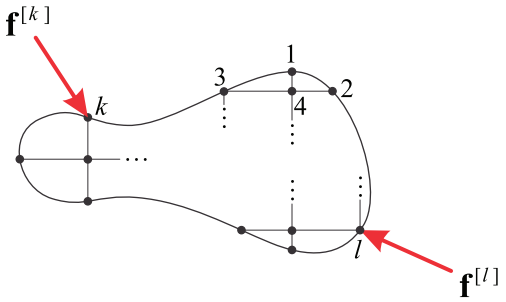

Figure A1 A structure under external forces.

Figure A2 Stinger model in axial direction.

where $\mathbf{x}^{[i]} = \{x_1{}^{[i]}, x_2{}^{[i]}, \ldots, x_n{}^{[i]}\}^{\mathrm{T}}$ and $\mathbf{f}^{[i]} = \{f_1{}^{[i]}, f_2{}^{[i]}, \ldots, f_n{}^{[i]}\}^{\mathrm{T}}$, respectively, are displacement and external force subvectors at node i, $\mathbf{S}^{[ij]} = (\mathbf{S}^{[ji]})^{\mathrm{T}}$ is dynamic stiffness submatrix between nodes i and j and T is the transpose operator. Global dynamic flexibility matrix, $\mathbf{H} = \mathbf{S}^{-1}$, from Eq. (A1) may be written in the form:

$$\mathbf{x} = \mathbf{H}\mathbf{f} \tag{A3}$$

where

$$\mathbf{H} = \begin{bmatrix} \mathbf{H}^{[11]} & \mathbf{H}^{[12]} & \cdots & \mathbf{H}^{[1m]} \\ \mathbf{H}^{[21]} & \mathbf{H}^{[22]} & \cdots & \mathbf{H}^{[2m]} \\ \vdots & \vdots & \ddots & \vdots \\ \mathbf{H}^{[m1]} & \mathbf{H}^{[m2]} & \cdots & \mathbf{H}^{[mm]} \end{bmatrix}$$

If external forces are only applied to nodes k and l, $\mathbf{f} = \{\mathbf{0}, \ldots, \mathbf{0}, \mathbf{f}^{[k]}, \mathbf{0}, \ldots, \mathbf{0}, \mathbf{f}^{[l]}, \mathbf{0}, \ldots, \mathbf{0}\}^{T}$, displacement vector at node k is obtained from Eq. (A2) as follows:

$$\begin{aligned} \mathbf{x}^{[k]} &= \mathbf{H}^{[kk]}\mathbf{f}^{[k]} + \mathbf{H}^{[kl]}\mathbf{f}^{[l]} \\ \mathbf{f}^{[k]} &= \mathbf{Z}^{[k]}\mathbf{x}^{[k]} - \mathbf{Z}^{[k]}\mathbf{H}^{[kl]}\mathbf{f}^{[l]} \end{aligned} \tag{A4}$$

where $\mathbf{Z}^{[k]} = (\mathbf{H}^{[kk]})^{-1}$. By the absence of external force at node l, $\mathbf{f}^{[l]} = \{\mathbf{0}\}_{n\times 1}$ In Eq. (A4), one may conclude:

$$\mathbf{f}^{[k]} = \mathbf{Z}^{[k]}\mathbf{x}^{[k]} \tag{A5}$$

Independent of motion in other nodes, $\mathbf{Z}^{[k]}$ in Eq. (A5) relates the displacement at node k to the only external force vector. Therefore, it is called dynamic stiffness matrix at node k.

Appendix II

While using the β excitation setup, the measured force with force transducer is not equal to the applied force on the SUT in axial direction of the excitation system. This unknown axial force can be calculated with the aid of the transfer matrix between two ends of stinger, q (force gage location) and p (attached point to the SUT), shown in Fig. A2. As the motion and forces in axial direction of stinger are independent of other DOFs, the transfer matrix between two ends of stinger can be written in the following form:

$$\begin{Bmatrix} x_1^{[q]} \\ f_1^{[q]} \end{Bmatrix} = \begin{bmatrix} T_{11} & T_{12} \\ T_{21} & T_{22} \end{bmatrix} \begin{Bmatrix} x_1^{[p]} \\ f_1^{[p]} \end{Bmatrix} \tag{A6}$$

where T_{ij} is element of the transfer matrix, $\mathbf{T}$. The second row of Eq. (A6) may be simplified in the form:

$$A_{11}^{[pp]} = \frac{T_{22}}{1/A_{11}^{[pq]} - T_{21}} \tag{A7}$$

where $A_{11}^{[pp]} = x_1^{[p]}/f_1^{[p]}$ and $A_{11}^{[pq]} = x_1^{[p]}/f_1^{[q]}$ are point and transfer FRFs, respectively. In order to find elements of the transfer matrix in above equation, two tests are done on the β setup. Forces, displacements and FRFs recorded from first and second test sets are marked with superscripts * and **, respectively. In the first test, excitation system is detached from SUT and $A_{11}^{*[pq]}$ is recorded. Because of the absence of external force at the point p (i.e. $f_1{}^{*[p]} = 0$), from the first row of the matrix Eq. (A6) one can conclude

$$T_{21} = \frac{1}{A_{11}^{*[pq]}} \tag{A8}$$

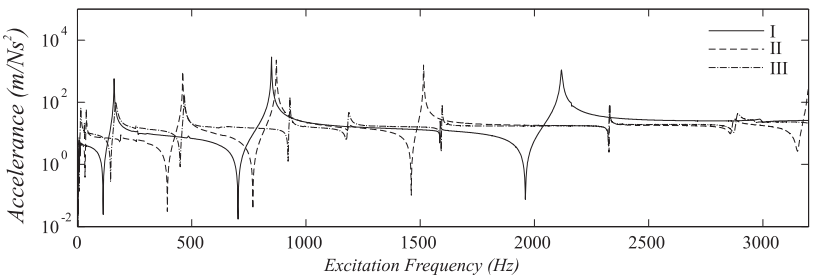

Figure A3 Measured FRFs of the SUT from the β setup.

In the second test, instead of the SUT, a particle with known mass of M is attached to the excitation system, and $A_{11}^{**[pq]}$ is measured. In this experiment, the external force exerted to the point p is ${f_1}^{**[p]} = -M\omega^2 {x_1}^{*[p]}$. Replacement of the measured quantities in the second row of the matrix Eq. (A6) leads to:

$$T_{22} = \left(T_{21} - \frac{1}{A_{11}^{**[pq]}} \right) / M\omega^2 \tag{A9}$$

Substituting Eqs. (A8) and (A9) in Eq. (A7), one obtains:

$$A_{11}^{[pp]} = \frac{A_{11}^{*[pq]} / A_{11}^{**[pq]} - 1}{M\omega^2 \left(1 - A_{11}^{*[pq]} / A_{11}^{[pq]} \right)} \tag{A10}$$

The above equation can be used to convert measured transfer FRF from β setup, $A_{11}^{[pq]}$, to point FRF $A_{11}^{[pp]}$. The measured direct transfer FRFs at points I, II and III with β setup are shown in Fig. A3 before converting them to point FRFs.